Bulletin of the Seismological Society of America, Vol. 96, No. 5, pp. 1915–1933, October 2006, doi: 10.1785/0120060119

Deriving Wavefield Characteristics and Shear-Velocity Profiles from Two-Dimensional Small-Aperture Arrays Analysis of Ambient Vibrations in a Small-Size Alluvial Basin, Colfiorito, Italy

by Giuseppe Di Giulio, Cecile Cornou, Matthias Ohrnberger, Marc Wathelet,* and Antonio Rovelli

Abstract We analyze the dispersion characteristics of ambient noise vibrations. For this purpose, two-dimensional (2D) seismic array data were acquired in four different sites in the Colfiorito plain, an alluvial intramountain basin that exhibits strong site effects. Assuming seismic noise being mainly composed of surface waves, we derive one-dimensional (1D) shallow shear-velocity profiles through the inversion of dispersion curves measured by frequency–wavenumber (*f-k*) methods. The inverted shear-wave velocity profiles are consistent with *a priori* information for those sites that can be approximated by 1D simple models. In these cases, the use of passive records of seismic vibrations can be a valuable tool for determining the shallow velocity profile if a detailed depiction of velocity structure is not required. The theoretical dispersion curves for Rayleigh and Love waves were compared with the measured dispersion curves for vertical and horizontal components, respectively. This allows us to discuss qualitatively the composition of ambient vibrations (outlining a large proportion of Love waves in the noise wave field) and the effects of higher modes. We also use the single-station method for investigating the origin of the horizontal-to-vertical (H/V) peak in the plain of Colfiorito in terms of ellipticity of the fundamental Rayleigh mode.

Introduction

The geotechnical characterization of the soil conditions is a crucial task for seismic hazard assessment. Very attractive tools for the determination of velocity and thickness of the soil layers are passive methods based on ambient noise recordings (Tokimatsu *et al.*, 1992). Such methods may indeed represent a low-cost and noninvasive exploration solution.

However, many issues concerning techniques based on ambient noise are still in debate within the scientific community. A research project (Site Effects Using Ambient Excitations [SESAME], 2001–2004) was recently financed by the European Community with the main purpose to clarify the nature of the ambient noise and to investigate the capability of noise-based techniques in retrieving relevant and quantitative information about the site features. In this article we discuss the results of one of the test sites chosen within the SESAME project (SESAME deliverable no. D06.05, http://sesame-fp5.obs.ujf-grenoble.fr/SES_TechnicalDoc.htm).

The study area is the Colfiorito plain, an alluvial basin of small size in central Italy (Fig. 1). Important site effects (Rovelli *et al.*, 2001; Di Giulio *et al.*, 2003) and the fairly well known geological structure of the basin (Fig. 1) are the two aspects that make this site attractive. We show the results of five small-aperture two-dimensional (2D) arrays deployed in the Colfiorito plain that recorded ambient vibrations. We analyze the variation of the resonance frequencies within the basin. Then we compute the phase-velocity dispersion curve for each array. The inversion of the dispersion curve, under the basic assumption that noise is composed of surface waves, provides near-surface shear-velocity profiles (e.g., Horike, 1985; Ohrnberger *et al.,* 2004a). Comparison between the inverted soil profile with the known geotechnical information allowed us (1) to assess the reliability of array techniques in estimating the local soil profile, and thereby (2) to check the adequacy of the starting assumption on noise composition. Finally, using the inverted shear profiles, we derive the theoretical one-dimensional (1D) site response.

For those sites with an available data set of local earthquakes, we find a good agreement between the theoretical and the empirical transfer function estimated through classical spectral ratio on the *S*-wave part of seismograms.

*Present address: Laboratoire de Géophysique Interne et Tectonophysique (LGIT/IRD), Grenoble, France.

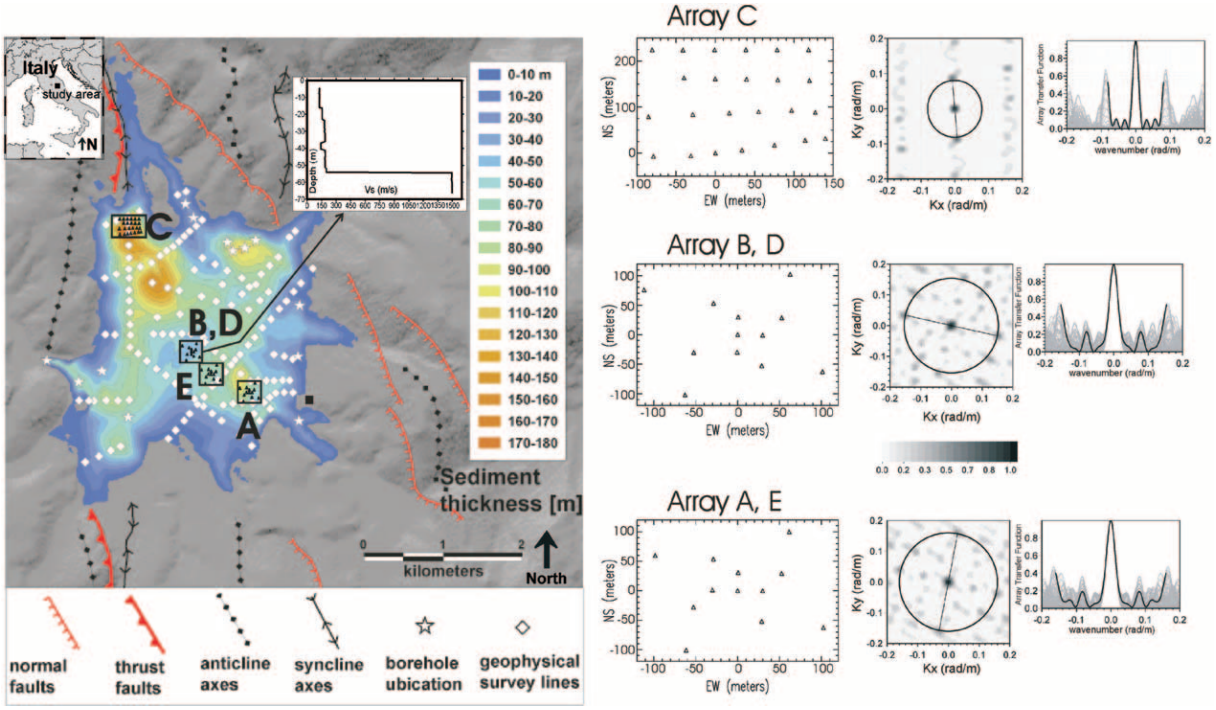

Figure 1. Left: Thickness of the low-velocity layer (silty-clayey sediments) (redrawn from Di Giulio *et al.* [2003]). The stamps show the location of the arrays. We reported the v_s profile from a downhole survey performed nearby where array B was deployed. Middle: Array geometry. Right: Array transfer function (ATF) for arrays C, B, and A. The black circle and black lines in the k_x-k_y plane show, respectively: (1) alias-lobe position when the ATF magnitude reaches a value of 0.5 (k_{alias}); (2) the direction when condition (1) occurs.

Colfiorito Basin and Array Layouts

The Colfiorito plain is a 3-km-wide intramountain basin in the Appenninic arc (Fig. 1). The plain is dedicated to agricultural activities. The sedimentary fill of the Colfiorito basin consists of alluvial deposits composed of lateral debris fans mixed with lacustrine sandy-clayey deposits. The alluvial sediment overlays a rock basement of limestone and marls of the Umbria–Marche Meso–Cenozoic sequence. The bedrock topography of the basin was inferred through boreholes and extensive seismic refractions and geoelectrical surveys (Fig. 1). The geomorphologic evolution of the study area is attributed to repeated occurrence of extensional earthquakes on a complex normal fault system aligned in northwest–southeast direction (Chiaraluce *et al.,* 2005). In this tectonic context, the two damaging mainshocks of 26 September 1997 (M_L 5.6 and 5.8 at 00:33 and 09:40 coordinated universal time [UTC], respectively) were located in close proximity to the Colfiorito plain and started the Umbria–Marche seismic sequence (Amato *et al.*, 1998). The earthquakes of the sequence recorded by stations deployed within the Colfiorito plain are characterized by a large amplification and duration of the seismic ground motion. Rovelli *et al.* (2001) and Di Giulio *et al.* (2003) analyzed the features of the recorded seismograms in the plain through 2D small-aperture arrays. These authors interpreted the long-duration ground shaking due to high-amplitude surface waves trapped and reverberating within the basin. They also estimated a shear velocity of 200 and 1200 m/sec for the sediment infilling and basement, respectively, by fitting the conventional spectral ratios with a simple 1D theoretical transfer function. In order to have more refined constraints on the local shear-velocity profile, downhole measurements were performed in June 2003 in the central part of the plain. The measured shear velocities are shown in the inset of Figure 1 confirming, on the average, the estimates empirically inferred from spectral ratios.

Within the scope of the SESAME project, a group of researchers of University of Potsdam and of Istituto Nazionale di Geofisica e Vulcanologia (INGV) installed in the Colfiorito plain temporary 2D seismic arrays to measure ambient noise. A set of homogeneous instrumentation was used, composed of MarsLite 20-bit digitizers and 3C Lennartz (Le3D-5s) sensors with an eigenfrequency of 0.2 Hz. The sampling rate and the gain were settled to 125 Hz and 2μV/count. The time synchronization was provided for each station by Global Positioning System (GPS) receivers (precision of 1 ppm). The positions of the receivers were determined using a differential GPS receiver (horizontal precision of about 0.5 m). All receivers were installed in free field and oriented to the geographic north. Some receivers were buried

in 40-cm-deep holes; the remaining sensors were installed on the ground surface after removing loose soil.

The location and configuration of the arrays are shown in Figure 1. Arrays A, B, D, and E were made of 12 receivers each. The layouts of these arrays are very similar: a central station surrounded by stations deployed on three rings with radii of about 30, 60, and 120 m with a number of three, four, and four receivers, respectively. A supplementary array (B_{large}) was obtained adding four stations in an outer ring of array B. Array D was deployed in the same configuration and position as B, the former recording mainly during the night, the latter recording mainly during the day. Array C was formed by 24 stations arranged in a rectangular configuration by four lines extending approximately along the east–west direction, with a station spacing of about 35 m. Additional details on the stations setting are listed in Table 1.

Arrays B, D, and E were deployed in the central part of the Colfiorito plain, where the interface between low- and high-velocity layer is relatively flat and where we expect 1D wave propagation. Arrays A and C were located above the southeast and northwest deeper bedrock sags, respectively, where the assumption of 1D wave propagation is not strictly verified. The whole experiment was carried out from 29 to 31 July 2002.

For the adopted layout we computed the array transfer function (ATF), defined as the array response for a vertically incident impulsive signal. In the wavenumber domain (k_x, k_y) the ATF quantifies the dependence of the aliasing on the azimuth (Fig. 1). We thus used the ATF to determine the performance of our array configurations (Woods and Lintz, 1973; Asten and Henstridge, 1984; Kind, 2002). We defined k_{alias} as the wavenumber distance between the main peak and the closest sidelobe exceeding 50% of main lobe magnitude (Fig. 1). In order to avoid alias effects, the maximum wavenumber resolution (k_{max}) of the array was defined as $k_{alias}/2$, while the radius of the main peak taken at its midheight provides the lowest wavenumber that can be resolved (k_{min}) (Fig. 1, Table 1).

We note that these definitions of k_{min} and k_{max} are within the range of the empirical indication of Tokimatsu (1997):

$$\frac{2\pi}{3d_{max}} < k_{min} < k_{max} < \frac{\pi}{d_{min}},$$

in which d_{min} is the minimum intersensor distance between receivers supposed to be equally spaced, and d_{max} is the maximum aperture of the array.

Single Station Horizontal-to-Vertical Analysis (of Array Stations)

For each receiver we calculated the spectral ratio between the horizontal and the vertical component of ambient noise (H/V) (Nogoshi and Igarashi, 1971; Nakamura, 1989, 2000). The frequency of the H/V peak at sites having a sediment-to-bedrock impedance contrast large enough approaches the fundamental resonance frequency of the soft layers (e.g., Lermo and Chàvez-Garcia, 1993; Lachet and Bard, 1994). Figure 2 shows the H/V curves computed through an antitrigger software implemented within the SESAME project (SESAME deliverable no. D09.03, http://sesame-fp5.obs.ujf-grenoble.fr/SES_TechnicalDoc.htm).

Arrays B and D, located at the same location and using

Table 1
Description of the Arrays

Array Name	Number of Stations (MarsLite + Le3d 5s)	d_{min} d_{max} (m)*	k_{min} k_{max} (rad/m)†	Starting Time (dd/mm/yyyy) (hr:min)‡	Ending Time (dd/mm/yyyy) (hr:min)‡	Remarks	f H/V (Hz)§
A	12	29.4 240.4	0.015 0.08	29/07/2002 09:43	29/07/2002 14:01		1.3
B	12	29.7 254.2	0.015 0.077	29/07/2002 13:04	29/07/2002 14:50		0.9
B_{large}	16	29.7 481.5	0.009 0.08	29/07/2002 14:50	29/07/2002 15:45	B + 4 stations added; but one of the stations was discarded for analysis due to an anomalous instrumental recording	0.9
C	24	34 304	0.01 0.04	30/07/2002 9:39	30/07/2002 12:46	The receivers along the two upper northern lines shows a flat H/V; for the two southern lines we observe a bumped H/V	
D	12	29.7 254.2	0.015 0.077	30/07/2002 15:52	31/07/2002 07:01	Same geometric configuration and position of B, but it recorded mainly during the night	0.9
E	12	29.4 240.4	0.015 0.08	30/07/2002 17:25	31/07/2002 06:58	Same geometric configuration of A	0.65

* d_{min} and d_{max} are the minimum interspace and maximum aperture between receivers, respectively.
† Range of resolution in terms of wavenumber (k_{min} − k_{max}) as defined by ATF.
‡ Period of the noise recordings.
§ Frequency of the H/V Peak.

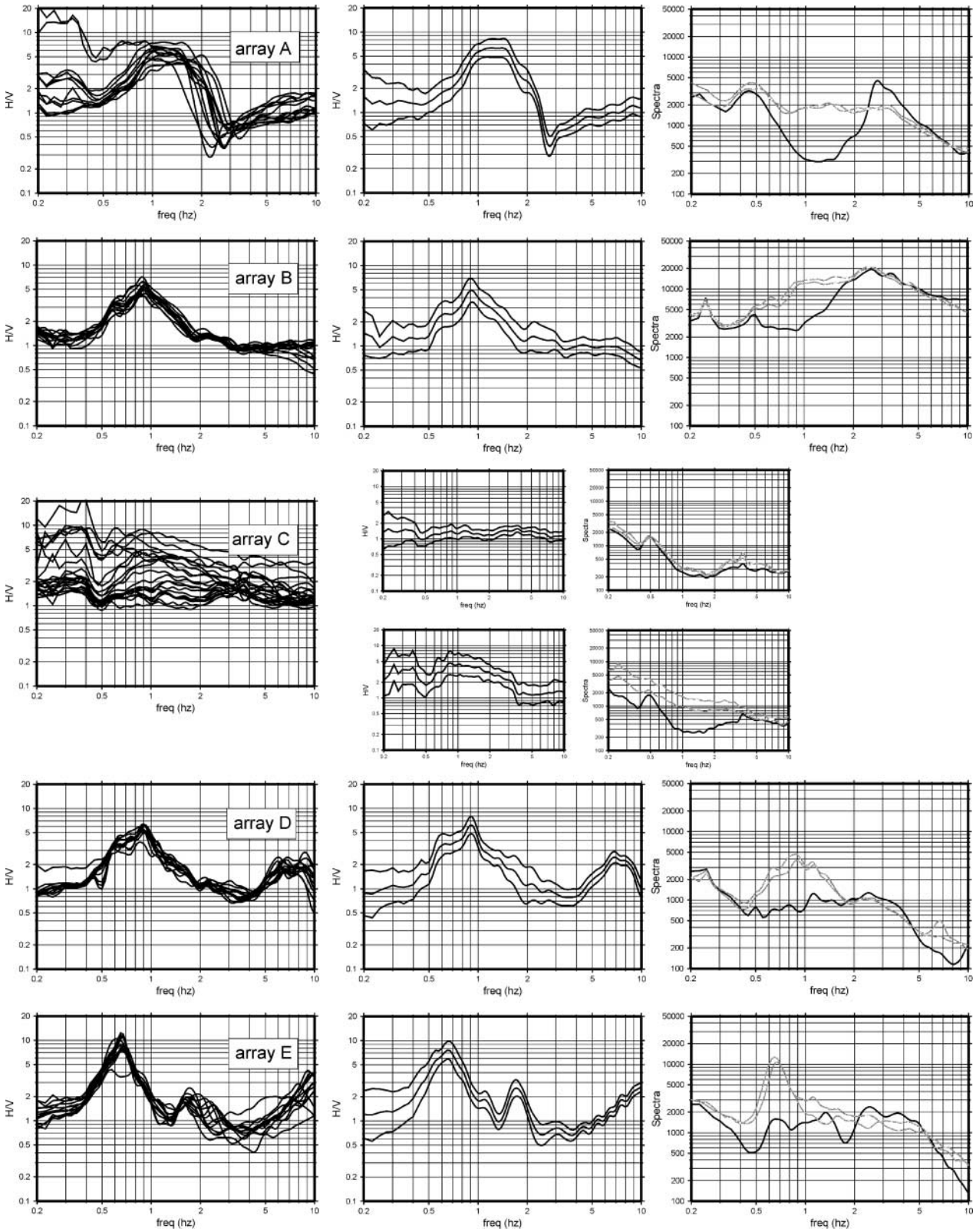

Figure 2. Left: We reported, for each individual station in the array, the mean H/V for 1-hr. recording processed by an antitrigger algorithm LTA/STA with a running time window of 40 sec. The LTA and STA were fixed to 25 and 1 sec, respectively. We applied the smoothing procedure of Konno and Ohmachi (1998) using a *b*-value of 40. Middle: H/V $\pm$ one standard deviation for 1 representative individual station. Right: Fourier amplitude spectra (arbitrary counts) of the three components for one representative individual station (the spectra of north–south and east–west component spectra are in gray; the spectrum of vertical component is in black).

recording data at different times, have a similar H/V with a resonance frequency of 0.9 Hz, the sediment thickness being around 50 m. However, we observe differences in terms of Fourier amplitude spectra of individual components starting from 1 Hz, probably due to the daily agricultural activities of the plain (Cara *et al.*, 2003). The array E, located about 250 m far away from arrays B and D, in an area where the depth of the sediment is about 65 m, exhibits a resonance frequency at 0.65 Hz. For array A, the H/V exhibits a broad peak around 1.3 Hz and a clear minimum of H/V amplitude around 2.5 Hz due to a maximum of energy on the vertical component.

The receivers of array C, in the vicinity of the deepest northwest depression (the maximum sediment thickness reaches 180 m), show the greatest variability in terms of H/V shapes among all the arrays. In particular, the stations of array C deployed along the two upper northern lines inside the array show a flat H/V over the entire frequency band, while the remaining stations exhibit a H/V composed of two broad bumps, at around 0.3 and 1 Hz, respectively (Fig. 2). This instability of the H/V between close stations can be regarded as an indicator of deviation from one-dimensionality caused by some peculiar local site effects, which will be discussed later. Recently, Bonnefoy-Claudet (2004) provided new insights on the nature of the H/V peak. This author generated noise synthetics for 1D models and tried an interpretation of the origin of the H/V peak in terms of the contribution of body (*SH/SV*) and/or surface waves (Rayleigh waves or the Airy phase of Love waves). The discriminating parameter resulting from these simulations is the impedance contrast between the soft sediment layers and the basement. When the impedance contrast is greater than 4 (as it is the case in Colfiorito) the H/V peak can be related to the horizontal polarization of the fundamental Rayleigh mode (see also Fäh *et al.*, 2001; Malischewsky and Scherbaum, 2004). The particle motion of ambient noise data in the frequency band around the H/V peak (Fig. 3) supports the interpretation of the H/V peak in Colfiorito in terms of ellipticity of Rayleigh waves.

Frequency-Wavenumber Analysis

The basic hypothesis of array methods used for estimating shear-wave velocity profiles is that the noise wavefield is mainly composed of surface waves (Tokimatsu, 1997). Rayleigh waves are assumed to be predominant (compared to body waves) in the vertical motion of the ambient noise, whereas in the horizontal plane Love and Rayleigh waves are mixed together (see particle motion in Fig. 3 in vertical and horizontal planes, respectively).

We used two different frequency–wavenumber (*f-k*) methods to determine the propagation characteristics of noise wave trains crossing the arrays. We processed the ambient vibration recordings with the conventional semblance-based frequency–wavenumber decomposition (CVFK) (Kvaerna and Ringdahl, 1986) and the high-resolution method (Capon, 1969).

The CVFK performs a grid search in the wavenumber plane (k_x, k_y) through a sliding time window analysis of filtered data in narrow frequency bands. The time delay for a plane wave propagating across the array is accounted for by applying phase shifts in the wavenumber domain. The most coherent plane wave provides the propagation characteristics (horizontal slowness s and azimuth θ):

$$\theta = \arctan\,(k_x/k_y)$$

$$s(\omega) = |\mathbf{k}|/\omega,$$

where $\mathbf{k}$ and ω indicate the wavenumber vector and the angular frequency, respectively.

In matrix notation, the *f-k* power spectrum estimator $\mathbf{P}(\mathbf{k}, \omega)$ can be expressed for CVFK method (we follow the notation of Zywicki [1999]) as

$$\mathbf{P}(\mathbf{k}, \omega) = \mathbf{e}^{\mathrm{H}}(\mathbf{k})\mathbf{R}(\omega)\,\mathbf{e}(\mathbf{k}).$$

Here $\mathbf{R}(\omega)$ is the cross-spectral matrix, $\mathbf{e}(\mathbf{k})$ indicates the steering vector that applies phase shifts associated with different trial $\mathbf{k}$, and $^{\mathrm{H}}$ denotes the Hermitian conjugate operator. When the steering vector is successful in aligning the array with plane waves propagating from a given direction and slowness, a peak in the estimator $\mathbf{P}(\mathbf{k}, \omega)$ occurs.

The Capon method computes the *f-k* cross-spectral matrix using a block averaging technique (Capon, 1969). The estimator is constructed such as (1) a plane wave with wavenumber $\mathbf{k}_0$ attempts to pass undistorted and (2) waves with wavenumbers $\mathbf{k} \neq \mathbf{k}_0$ are minimized in a least-squares sense. For the Capon method the *f-k* power spectrum estimator $\mathbf{P}(\mathbf{k}, \omega)$ is defined as

$$\mathbf{P}(\mathbf{k}, \omega) = 1/\left[\mathbf{e}^{\mathrm{H}}(\mathbf{k})\mathbf{R}(\omega)^{-1}\,\mathbf{e}(\mathbf{k})\right].$$

The Capon and CVFK techniques differ basically in the choice of the spatial weighting scheme. The Capon method has a higher angular resolution than the CVFK technique, allowing a better resolution of waves propagating at close wavenumbers. However, the Capon method is found to be in some cases less robust than CVFK and does not allow a statistical analysis of the results (Zerva and Zhang, 1996; Ohrnberger *et al.*, 2004b; Wathelet, 2005).

The analysis software was implemented within the framework of the SESAME project; we refer for details to the article by Ohrnberger (2004) and Ohrnberger *et al.* (2004b). The most appropriate processing parameters were selected after different tests on field and synthetic data (SESAME deliverable no. D07.05, http://sesame-fp5.obs.ujf-grenoble.fr/SES_TechnicalDoc.htm).

We measured the wave-propagation characteristics using 200 frequency bands in the range 0.2–4 Hz. The lower frequency of analysis is given by the eigenfrequency of the

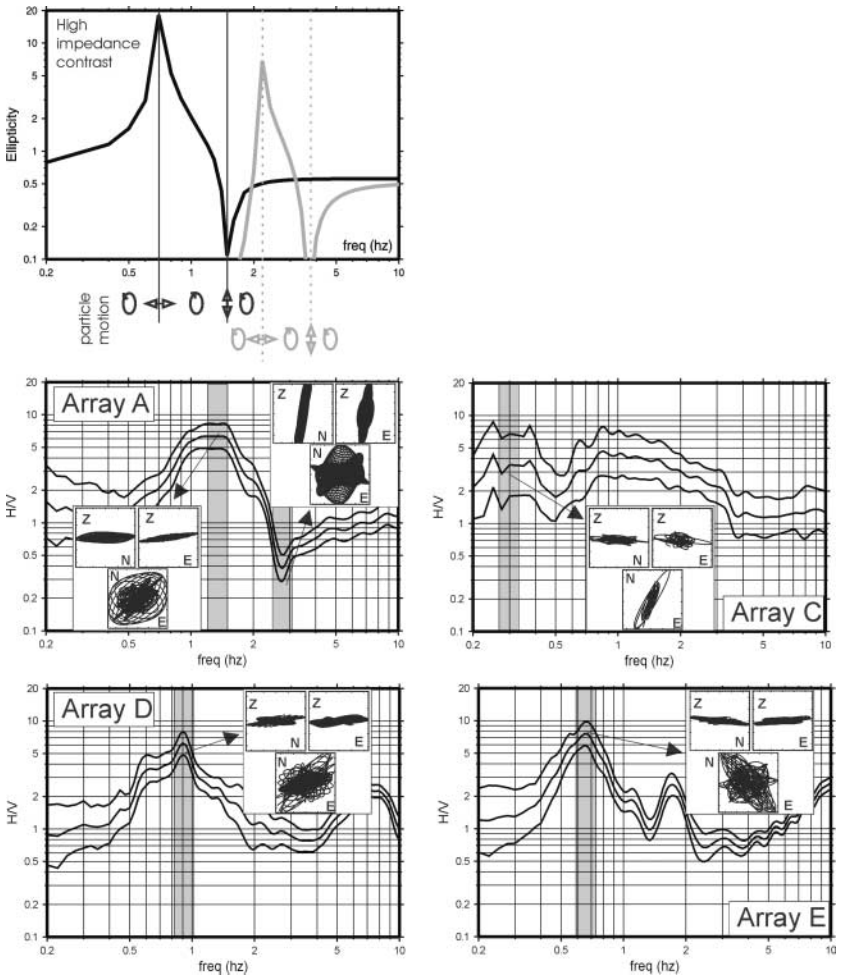

Figure 3. Top: Ellipticity of the fundamental and first higher Rayleigh-wave modes computed for a single layer over half-space having a high-impedance contrast (>4) (after Bonnefoy-Claudet, 2004). Bottom: Particle motion computed in the horizontal (NE) and vertical plane (ZN, ZE) for 60 sec of noise recordings previously bandpass filtered around the H/V peaks (gray area). Note that in the vertical plane the polarization is typical of Rayleigh waves.

sensors; the upper frequency is given by the spatial aliasing. The central frequency f_c for each band was selected to be logarithmically spaced. A fraction of the central frequency f_c defined the frequency bandwidth ($0.9f_c - 1.1f_c$). We selected the time-window length as 20 times the central period corresponding to the analyzed frequency band f_c and used an overlap of 50% between successive time windows. The wavenumber domain was scanned by a search on a polar grid uniformly sampled in slowness and azimuth (sampling set to 25 sec/m and 5°, respectively).

Dispersion Curves and Backazimuth

We computed the dispersion curves for each array using 20 min of noise recording. In order to verify the consistency of the results, we applied two *f-k* techniques previously discussed (CVFK through a sliding time window and Capon using a block-averaging technique for computing the *f-k* cross-spectral matrix). We selected the noise data to process after a visual control of the waveforms and of the corresponding Fourier amplitude spectra quality for all the array stations. When possible, we analyzed time windows recorded simultaneously by different arrays (Table 1). Figure 4 shows the dispersion curves obtained using the vertical component of seismic noise.

As already mentioned, the frequency range where the dispersion curve is reliable depends on the effective wavelengths contributing to the wave field and the limitations induced by array geometry (minimum and maximum resolvable wavelengths). Wathelet *et al.* (2004) stressed, however, the difficulty in finding the valid frequency ranges when empirical rules are adopted. Scherbaum *et al.* (2003) focused their attention on the vanishing of the vertical motion energy in correspondence to the resonance frequency caused by a filter effect of the sedimentary layer. Following the indication of the above mentioned articles, we defined the upper frequency limit as the intercept of the dispersion curves with the aliasing curve $v = 2\pi/k_{max}\, f$ (where v is phase velocity, f is frequency, and k_{max} is maximum wavenumber defined from ATF); whereas the lower limit was fixed around the local resonance frequency of the sites. This lower limit is close to $k_{min}/3$ (see Fig. 4) in agreement with the experimental results found by Asten and Henstridge (1984) and Horike (1985).

In this frequency range, the Capon and CVFK methods provide a similar estimate of phase velocity for arrays *B,*

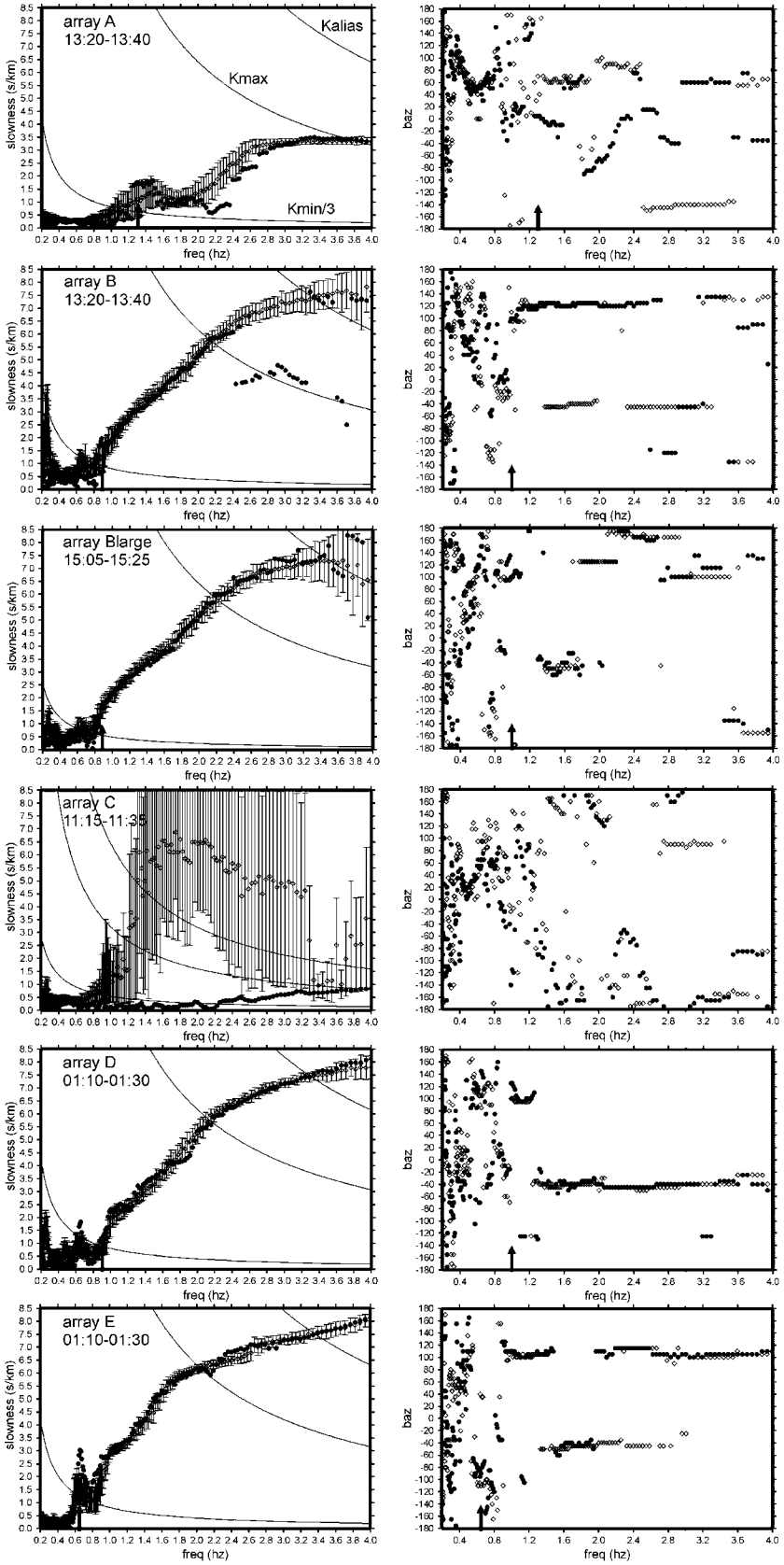

Figure 4. Left: Dispersion curves obtained for vertical component by both *f-k* methods. The diamonds with bars represent the results obtained by the CVFK method (median and its standard deviation for the complete ensemble of slowness estimates). The black circle is the dispersion curve obtained for the Capon method (we plotted the first highest maximum of *f-k* estimator). We overlaid the aliasing curves for k_{alias}, k_{max}, and $k_{min}/3$. In the corner we indicated the time window processed. Right: Backazimuth distribution (in degrees clockwise from the north) obtained using the CVFK and Capon methods (white diamonds and black circles, respectively). The arrow on the axis of the frequencies indicates the position of the H/V peak ($f_{H/V}$, see Fig. 2).

B_{large}, *D*, and *E*. Larger differences between the apparent slownesses obtained by the two methods are observed for array *A*. The branch at higher frequencies of the dispersion curves contains information on the shallower part of the soil. The superficial layer is characterized by similar values of slowness for arrays B, B_{large}, D, and E (6.5 sec/km, i.e., 150 m/sec); this value of velocity is in agreement with the shear-velocity profile derived from downhole measurements. On the contrary, the measure of slowness for array A obtains larger velocity (3 sec/km, i.e., 330 m/sec). The only case where the two *f-k* methods provide very different results is for array C.

The backazimuth distribution (Fig. 4) shows scattered values below the resonance frequencies of the sites where the arrays do not have penetration capabilities. Above, predominant stable directions can be observed, in particular $-50°$ and 110° clockwise from north at the arrays located in the central part of the plain (B, D, E). Comparison of backazimuths observed within the same time window (array D and E, and array A and B) at nearby arrays suggests some persistent directions that could be related to close sources and/or stable reverberating waves scattered from outcrop edges or linked to the irregularities of the bedrock topography. Comparison of backazimuths observed at arrays B and D deployed at the same location but at different time periods suggests that some directions are not persistent in time and could be ascribed to the anthropic daily activities.

Persistent similar backazimuths of 110° and $-50°$ N were already observed in previous studies using local earthquakes data (Rovelli *et al.*, 2001; Di Giulio *et al.*, 2003); these directions were associated to a nearby rock outcrop (east-southeast of array A) and to the deepest depression of the bedrock topography (northwest of array B), respectively. Maresca *et al.* (2006) found similar predominant directions on noise propagation using array techniques applied to the data set of arrays A and B.

In order to investigate the robustness of our results we measured the propagation characteristics of the noise wave field for several time windows at arrays D and E. Figure 5 shows that dispersion curves are very stable in time. Noise wave trains propagating at lower slowness could be associated to higher modes, especially for array E (see Fig. 5). The backazimuths distribution confirms the presence of distinct wavefield directions that seem to exhibit a dependence with time.

For array C we tried to process only the stations deployed along the two southern lines (see Figs. 1 and 2), excluding the stations that show a flat H/V curve. The two *f-k* methods return still ambiguous results as displayed in Figure 4. According to the lateral confinement of the deep sag in the vicinity of array C (width of about 500 m and maximum thickness of 180 m), some three-dimensional (3D) local resonance effects are expected (Rial, 1989). These effects are more complex and difficult to extract than 2D resonances in embanked valleys (Bard and Bouchon, 1985; Roten *et al.*, 2004). This complication does not allow clarification of the wave-propagation type within this area of the basin and prohibits the interpretation of array analysis results for array C.

Velocity Profiles from the Inversion

The dispersion curves computed with *f-k* methods were inverted to 1D-layered velocity models using the neighborhood algorithm (Sambridge, 1999) as implemented by Wathelet *et al.* (2004). The neighborhood algorithm performs a stochastic search of the parameter space, that is, body-wave velocities (v_p and v_s) and the thickness and the density of the soil layers. As input of the inversion algorithm, we considered the measured dispersion curves of the vertical ambient vibration component within the usable frequency range ($k_{min}/3 - k_{max}$) previously discussed.

The parameterization of the soil model was achieved using a single layer overlaying half-space. The upper layer represents the soft sediment and is modeled as a stack of five sublayers following a power law velocity with depth. The valid parameter ranges for the sampling of velocity models are given in Table 2. In order to not limit the number of possible solutions, we allowed a quite large range of v_s and thickness (Table 2). Because v_p velocities poorly constrain Rayleigh-wave phase velocities (Xia *et al.*, 1999), we limited the v_p to 1000–1300 m/sec, and we fixed it to 2400 m/sec for the upper sediment layer and the half-space, respectively. These values are consistent with the results of seismic refraction profiles carried out in the plain of Colfiorito (Congeo l.t.d., unpublished report, 1998). For sake of simplicity we consider only the fundamental mode in the inversion procedure. In the forward computation more than 5000 1D models associated to the fundamental Rayleigh-wave mode were generated in the attempt to fit the measured slowness curve.

Figure 6 shows the resulting v_s profiles obtained by the inversion and the associated fundamental Rayleigh-wave dispersion curves. The observed phase-velocity curves are in general well fitted by the dispersion curves associated to the theoretical fundamental Rayleigh-wave mode. This is particular true for arrays B, B_{large}, and D (same site), where we obtain very similar results (see Fig. 6). It is interesting to note that we obtain slightly better fits between measured and inverted dispersion curves for the night recordings (array D). For arrays A and E the observed jumps in narrow frequency bands (1.5–2.0 Hz and 0.8–1.0 Hz, respectively) cannot be satisfactorily explained by the fundamental Rayleigh-mode assumption and could be explained as effect of the higher modes (Tokimatsu *et al.*, 1992; Tokimatsu, 1997; Forbriger, 2003) or in terms of low energy of the surface waves in the vertical component.

According to the known sediments-to-bedrock interface depth (see the reconstruction of the buried bedrock topography in Fig. 1), the sediment thickness is estimated quite satisfactorily for arrays B, B_{large}, D, and E. In contrast, for array A an inverted depth of about 60 m underestimates the

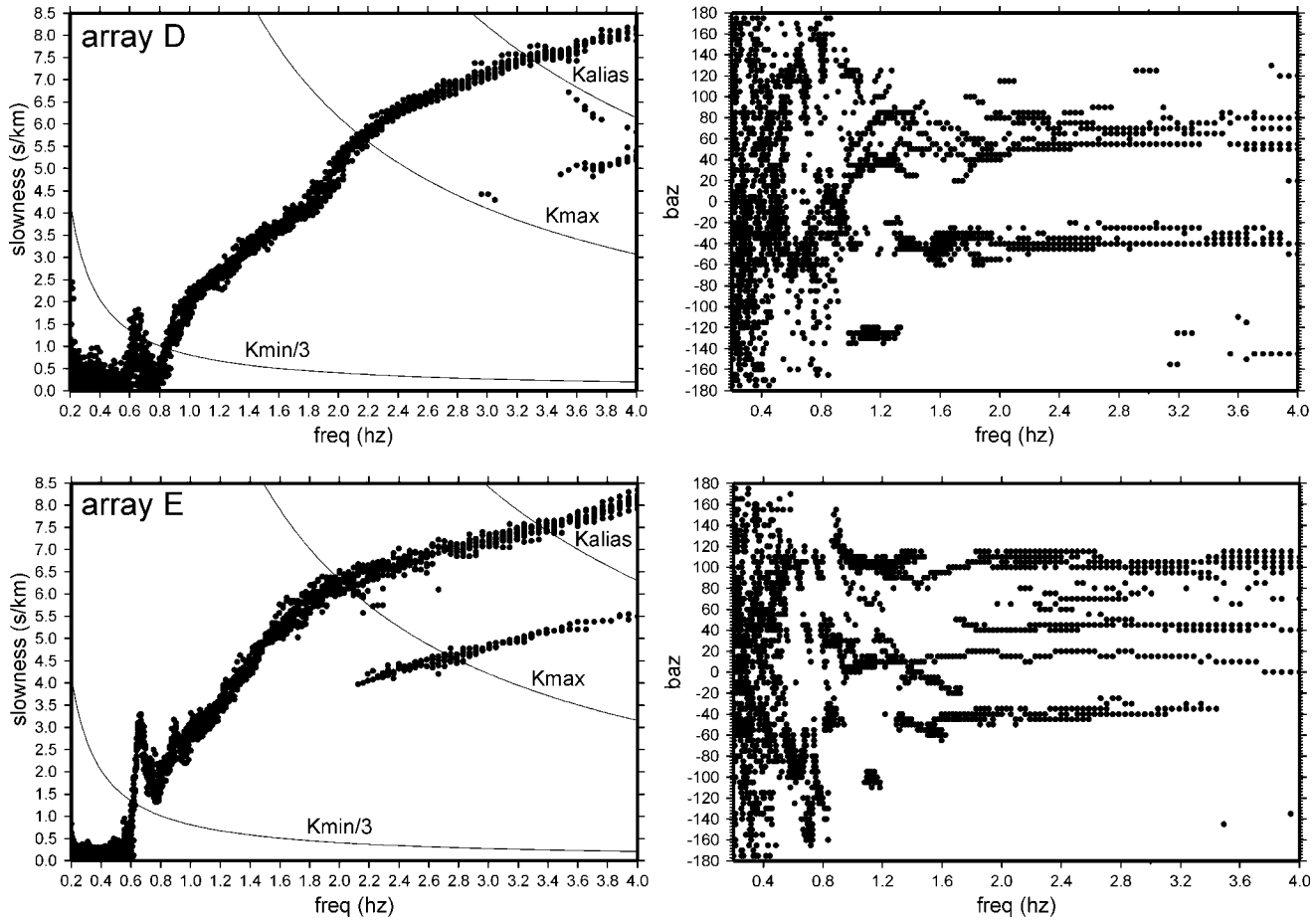

Figure 5. Dispersion curves and backazimuth distribution computed using the Capon method for 13 subsequent time windows of 20-min duration each: the first time window is 18:20–18:40, the second time window is 19:20–19:40, . . . and the last time window is 06:20–06:40. We overlaid the k_{alias}, k_{max} and $k_{min}/3$ aliasing curves.

Table 2
Allowed Parameter Range for the Searching of the Parameter Space in the Inversion Procedure

Thickness (m)	v_p (m/sec)	v_s (m/sec)	Number of Sublayers Allowed
20–200	1000–1300	100–600 400–1700	5

The density was fixed to 1.9 and 2.3 g/cm^3 for the soft and basement layer, respectively. The v_p value was fixed to 2400 m/sec for the basement layer.

average value (about 80 m) of the sedimentary thickness below the receivers as inferred from Figure 1.

The inverted shear-wave profiles for the sediment infilling at arrays B, B_{large}, D, and E are in quite good agreement, in terms of average value of v_s, with the downhole shear-wave profile available in the central part of the plain (error lower than 10%; see Table 3). A fine reconstruction of the topmost soil was not possible because the array apertures and the intersensors distances were too large to properly capture the high frequency (>4 Hz) wavefield properties.

For array A, which is located approximately at a distance of 750 m and 450 m from arrays B and E, respectively, the inversion indicates larger velocities for the superficial soil (see Fig. 6, Table 3). We suspect that these larger velocities (deviation of 80% compared to the shear-wave velocity estimated in the middle of the basin) are related to a more complex layering (we will discuss this feature later).

The inverted bedrock structure obtained for all the sites shows a quite large variability of shear velocity (800–1700 m/sec) due likely to the lack of resolution induced by the limited aperture of the arrays and/or the lack of energy on the vertical component at frequencies smaller than the resonance frequency of the sites (Scherbaum *et al.*, 2003).

Horizontal Components

Among all the inverted models obtained from the analysis of the vertical components (see Fig. 6), we selected for

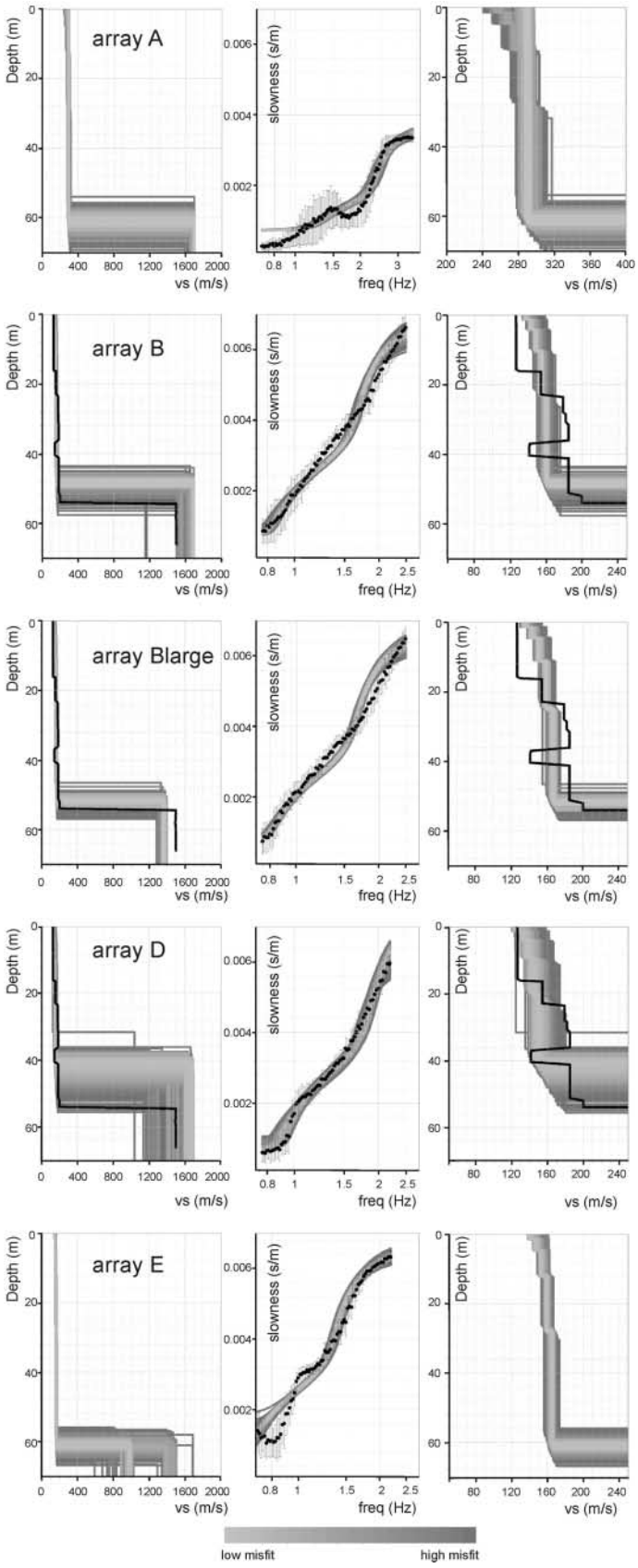

Figure 6. From left to right for arrays A, B, B_{large}, D, and E: v_s inverted profiles, the black line indicates the v_s profile derived from downhole measurements (arrays B, B_{large} and D) when available; dispersion curves obtained after inversion overlaid by the observed phase velocity for the vertical component estimated using the CVFK method (black circles and relative standard deviation); zoom of the v_s inverted profiles for the upper layers overlaid by the v_s derived from downhole measurements (black line). The tonalities of gray are proportional to the misfit carried out by the inversion.

Table 3
Comparison between the Downhole Measurement and the Results Obtained by Inversion for the Best Model of Figure 6 (Lowest Misfit Value)

	v_s Soft Layer (m/sec)	Δ (%)	v_{s30} (m/sec)	Δ (%)	v_s Basement (m/sec)	Δ (%)	Thickness of Soft Sediment (m)	Δ (%)
Downhole	161		146		1497		54	
Array A	290	+80	290	+99	1697	+13	61	+13
Array B	161	0	153	+5	1694	+13	48	−11
Array D	144	−10	142	−3	1677	+12	41	−24
Array E	160	0	156	+7	977	−35	61	+13

We reported the average of the shear velocity for the soft layer, for the topmost 30 m, for the rock basement, and the thickness of soft-bedrock interface. The velocity values are weighted using the thickness h_i of the sublayers ($v_s = \sum_i v_{si} \cdot h_i / \sum h_i$). The symbol Δ indicates the deviation from the downhole measurement carried out in the middle part of the plain (see Fig. 1).

each array the model that provided the lowest misfit (i.e., smallest distance between theoretical and experimental dispersion curve). For this best model we computed the theoretical Rayleigh and Love dispersion curves of the fundamental mode (R and L hereinafter) and the ellipticity curve (Fig. 7). Then we processed the two horizontal components of our recordings by *f-k* analysis in order to measure phase velocity. Because the apparent phase velocities measured using north–south and east–west components are very close, we calculate the average phase velocities in the horizontal plane. If Rayleigh and Love waves are equally contributing to the noise wave field, the effective Rayleigh- and Love-phase velocities should lead to phase velocities in between the related theoretical dispersion curves (Cornou *et al.*, 2003). On the contrary, if one of the surface-wave types dominates the wave field, it is expected to measure phase velocities close to the actual phase velocity of this surface wave. The results are shown in Figure 7. Arrays B and D show a good match between measured and theoretical dispersion curves: vertical and horizontal components are well fitted by R and L, respectively. This finding is a strong indication that the Rayleigh waves are predominant in the vertical plane and Love waves dominate the noise wave field in the horizontal plane. For array E, we observe a probable higher mode effect in the horizontal plane starting from 1.5 Hz (higher mode is also expected for Rayleigh waves, as suggested by Fig. 5).

The ellipticity of the theoretical fundamental mode of Rayleigh waves provides similar results in terms of frequency of H/V peak, confirming the conclusion inferred from polarization analysis (Fig. 3) on the origin of the H/V peak in Colfiorito. For array B, where we obtained a good fit between effective and theoretical dispersion curves, we performed an additional test (by courtesy of Donat Fäh) by inverting only the ellipticity information. The resulting shear-wave velocity is consistent with the result obtained by inversion of the dispersion curves (the deviation from the value of downhole measurement is less than 10% in terms of average shear velocity and thickness of soft layer). This test suggests that the use of a single station in providing the soil profile can be appropriate in simple 1D sites characterized by a strong impedance contrast (Fäh *et al.*, 2003; Arai and Tokimatsu, 2004).

For array A the comparison between theoretical and experimental dispersion curves (Fig. 7) suggests that Rayleigh waves completely dominate the noise wave field. In particular the H/V shape for array A exhibits an ideal Rayleigh-wave ellipticity with a minimum at 2.5 Hz (Fäh *et al.*, 2001), but we observe at the resonance frequency that the H/V peak is less sharp than the H/V peaks of the other arrays.

Reliability of Shear Velocities Estimated at Array A

As previously mentioned, a larger shear velocity of the alluvial infilling compared to the one in the middle of the basin was estimated at array site A (290 m/sec versus 160 m/sec, see Table 3). Such shear velocity could be apparent and produced by energetic higher modes that propagate at higher phase velocities than the fundamental mode at the same frequency (Tokimatsu *et al.*, 1992). Alternatively, larger values could be due to a real increase of v_s in this part of the basin. This ambiguity for array A is now investigated considering in more detail the geological and geophysical available information. In the vicinity of array site A, which is located near the southeastern edge of the basin, Chiaraluce *et al.* (2005) recently inferred through a geological study the presence of a superficial deposit composed of alluvial fan coming from the erosion along preferential drainage patterns of nearby limestone outcrops. Observations of Chiaraluce *et al.* (2005) are supported by the results of a geoelectric survey performed close to array site A. The resistivity data in Figure 8 shows indeed a significant accumulation of a superficial layer (about 20 m of thickness) of high resistivity (200–300 ohm m) and likely of high compactness overlaying the clay low-velocity layer (with resistivity values of 5–20 ohm m, typical of clays in the region). Beneath array A, the resistivity model shows an interface depth between infilling and basement at 80 m on the average.

The presence of a soft layer trapped between stiffer ones may modify the wave propagation and the relative contribution of fundamental and higher modes in the noise wave

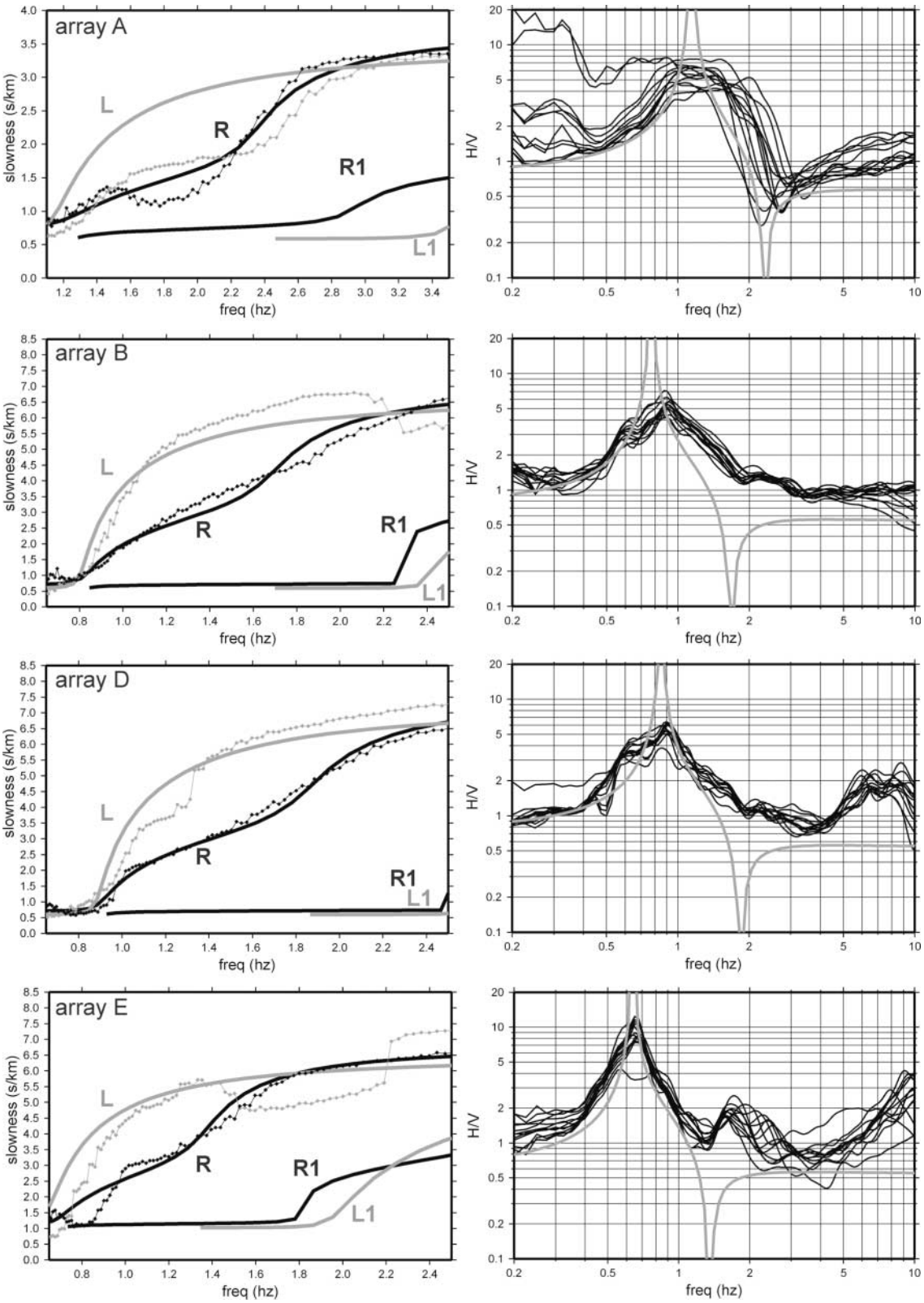

Figure 7. Left: Observed dispersion curves for vertical and horizontal motion (black and gray thin lines, respectively). The dispersion curve for horizontal component was obtained by averaging the dispersion curves computed separately on the north–south and east–west components. From the best models in Figure 6 we overlaid the theoretical Rayleigh and Love dispersion curve for the fundamental and first mode (black and gray thick lines marked with R/R1 and L/L1, respectively). Right: Ellipticity curves for the best model in Figure 6 overlaid by the H/V curves.

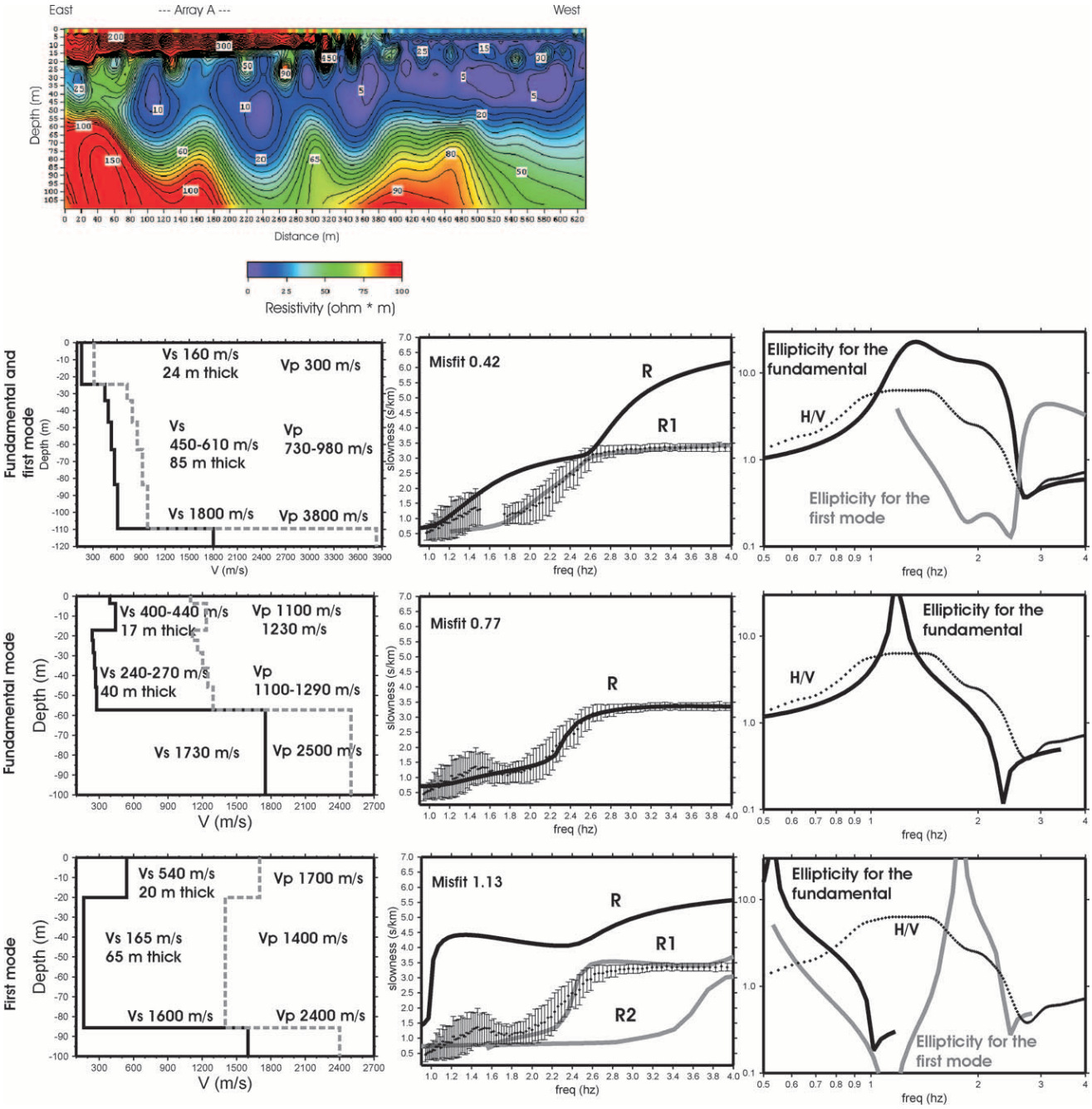

Figure 8. Top: Resistivity model obtained from a multieletrodic profile (using a line of 64 electrodes with a spacing of 10 m). The projection of the array A position is reported. Numbers indicate the values of resistivity (ohm m). Bottom: V_p and V_s velocity profiles, dispersion curves, and ellipticity corresponding to the best inverted model assuming three layers and the following scenario: simultaneous inversion of the fundamental and the first mode; inversion of the fundamental mode; inversion of the first higher mode. The measured dispersion curve (diamonds and relative standard deviation) and the computed H/V (diamonds) are overlaid.

field. In order to analyze how such superficial deposit may affect the wavefield propagation, we repeated the inversion of the dispersion curve for array A using a more refined model parameterization allowing three layers (two main soft layers above basement).

We have analyzed the following three cases: (1) simultaneous inversion of the fundamental and the first Rayleigh-wave mode, (2) inversion considering only the fundamental mode, and (3) inversion considering only the first mode. In the first case, based on the shape of the measured dispersion

curve for the vertical component, we simultaneously fitted the lower frequency range of experimental data (1–1.5 Hz) as fundamental mode and the higher frequency range (1.75–4 Hz) as first mode. The data in the range 1.5–1.75 Hz were not used in the inversion because they were assumed to be mixed between the fundamental and the first higher mode.

In order to obtain a solution from the inversion, a larger range of free parameters compared with Table 2 was needed. Among all the inverted models, a single representative model characterized by the lowest misfit was extracted, and for this best model the theoretical ellipticity was computed. Figure 8 shows the results. Using the simultaneous multimode inversion (fundamental and first higher modes), the best model indicates a first layer with low v_s values (160 m/sec) overlaying a second layer with larger values of v_s (450-610 m/sec). The depth of soft-basement interface in this model is slightly overestimated (109 m versus 80 m). The misfit is very low (0.42), and the ellipticity curve derived for this inverted model fits fairly well the actual H/V curve. Nevertheless, the result is questionable because the increase of v_s with depth contradicts the expectation based on geoelectric data.

When only the contribution of fundamental mode is assumed, the match of theoretical and experimental dispersion curves is very good within the range 1.6–4 Hz. The misfit (0.77) is acceptable. The most superficial layer is characterized by v_s of about 420 m/sec. The shear velocity of the second layer exhibits a velocity (about 260 m/sec) similar to the one estimated by considering only a two-layer model in the inversion (290 m/sec., see Table 3). The depth of the sediment-to-bedrock interface is only partially approached (57 m versus 80 m). The theoretical ellipticity matches very well the actual H/V curve, especially the fundamental frequency and the first trough at 2.5 Hz.

Among all the cases, the worst match between estimated and experimental dispersion curves (highest misfit, 1.13) is obtained when the first mode is assumed to be the most energetic one. The shear velocity of the layer between the uppermost high-velocity layer and the basement exhibits low shear-wave velocity (165 m/sec). This value is consistent with the average v_s derived at arrays in the middle of the basin (see Table 3). The depth of the sediment-to-bedrock interface is also realistic (85 m). However, features of the actual H/V are not reproduced, which makes this model unlikely.

Based on the results of the scenarios considered in Figure 8, our preferred velocity model class is the one obtained considering the contribution of the fundamental mode only. This velocity profile shows a velocity reversal that is consistent with the resistivity data. Furthermore, the agreement between the H/V curve and the ellipticity is rather good. The available geological and geoelectric information as well as the different inversions of Figure 8 suggest that, close to the southeastern edge of the basin, a different process of sedimentation yielded to a rather complex velocity structure and probably to values of v_s within the alluvial infilling larger than in the central part of the plain (250–290 m/sec versus 160 m/sec). However, the contrasting near-surface velocity profiles shown in Figure 8 are a significant example of how the identification of the modes is a very crucial step. This is in general true for all the seismic surface-wave methods that estimate first a dispersion curve and then derive the shear-wave velocity profile through an inversion algorithm. The reliability of the inverted model depends on the wave propagation phenomena being modeled correctly in the inversion. A correct identification and interpretation of modes improves the accuracy of the inverted model (i.e., Xia *et al.*, 2003), whereas an inappropriate discrimination of modes can produce an inverted model far from the real one. Unfortunately, there is no independent objective procedure for automatic discrimination between modes based on the observation only. Mode identification is usually determined visually by experience observers or justified *a posteriori* from comparison to forward models. From the shape of the dispersion curve measured at array A we determined the frequency range where a change of the contribution of energy from the fundamental mode to an energetically dominating first higher mode could be expected. The number of possible model classes would increase if the separation between modes is not held fixed but is allowed to vary within a larger frequency range. The different modes concentrate in different frequency bands depending on the local structure. Higher modes are expected to be excited in complex layered sites, for example, profiles where a strong velocity inversion occurs. In order to assess a more complete dispersion curve in this kind of site, the ambient noise techniques could be integrated with multichannel methods that involve simple active sources (i.e., Multi-Channel Analysis of Surface Waves [MASW]) (Park *et al.*, 1999). Due to the relatively low frequency content of microtremor, the strength of ambient vibration array techniques lies in the derivation of intermediate to deep structures (hundreds of meters). The assumption that only Rayleigh waves are measured is particularly less fulfilled for passive techniques than for active ones: body-waves interferences or lack of energetic surface waves in ambient wave field generally result in a high uncertainty in the estimation of phase velocity. In contrast, methods using small active sources provide more precise velocity estimates within the dedicated frequency range, which is located at higher frequencies than for ambient vibration techniques. Hence higher modes, usually developed at high frequency where they can carry more energy than the fundamental mode, are often observed with active experiments as reported in the literature (e.g., Park *et al.*, 1999; Jin *et al.*, 2006). In principle, instead of the adoption of passive techniques alone, an integrated approach of passive and active techniques could allow investigation of the dispersion properties in a broader frequency range and better identification of higher modes.

Earthquake Coda

During the deployment of array D, we recorded a local earthquake (M_d 2.5, epicentral distance 8 km) at seven sta-

tions. Within the assumption of earthquake coda being composed by surface-diffracted waves (Aki, 1969) propagating in the plain, we processed this event by *f-k* methods excluding direct *P* and *S* waves (Fig. 9). We adapted the processing parameters for taking into account the short duration of the time window and the signal-to-noise ratio. We measured the propagation characteristics using 200 frequency bands in the range 0.8–3.0 Hz. We fixed the time-window length as 8 times the central period corresponding to the analyzed frequency band f_c; this choice with an overlap of 50% allowed the computation of the propagation characteristics averaged over 5 windows for the lowest frequency. Then we compared the results between the coda earthquake and a part of noise recording of equal time length (30 sec). The dispersion curves measured from the horizontal motion shown in Figure 10 indicate a nonnegligible contribution of Love waves in the horizontal plane for ambient vibration records as well as earthquake-coda signal. However, some differences in the behavior are observed, probably due to a different proportion between surface and/or body waves in the two cases (coda and noise). The horizontal component exhibits a larger slowness value for the noise data; the vertical component of the earthquake coda provides a rather constant value of horizontal slowness (~3 sec/km) in a broad frequency band (1–1.75 Hz). Because the earthquake is a far-distant and deep source relative to the basin, this nondispersive feature of the coda signal could be due to the contribution of multiple diffracted waves by regional heterogeneities (Schisselé *et al.*, 2004).

Even though only one earthquake can be analyzed, the general trend of the dispersion curves for both horizontal and vertical components between noise and coda earthquake is quite similar. This result corroborates that the use of ambient noise is appropriate for getting a valid representation of the actual wave propagation and medium properties.

Conclusion

The methods based on ambient noise recordings have gained increasing interest over the last decade because of their low cost and relative simplicity of use. The H/V single-station method can provide the resonance frequency of the soil, which is for 1D structures closely related to the thickness and the velocity of the soft soil. The array techniques can be used to measure the dispersion characteristics of the noise wave field. These two techniques are strictly correlated and can be complementary (Scherbaum *et al.*, 2003; Fäh *et al.*, 2003). Parolai *et al.* (2005) retrieved a more reliable shear-velocity profile for a real site using a joint inversion of phase-velocity dispersion and H/V ratio curves.

The building codes for seismic design usually adopt the averaged shear velocity of the topmost 30 m (v_{s30}) soil as the main discriminating parameter for classification of soil classes (e.g., Dobry *et al.*, 2000; Building Seismic Safety Council, 2001). Techniques based on surface-wave theory are very attractive for the estimation of the shallow subsurface structure; they basically derive the soil profiles by means of inversion of the phase-velocity dispersion curves. In principle, the apparent phase velocity can be measured by receivers arranged in an appropriate geometry on the ground surface using active (i.e., SASW) (e.g., Stokoe *et al.*, 1994; Brown *et al.*, 2002) and passive sources. In a recent study by Asten and Boore (2005), a blind comparison of the subsurface shear-velocity profiles from different invasive and noninvasive methods was performed. These authors showed that reliable results are obtained when ambient vibration ar-

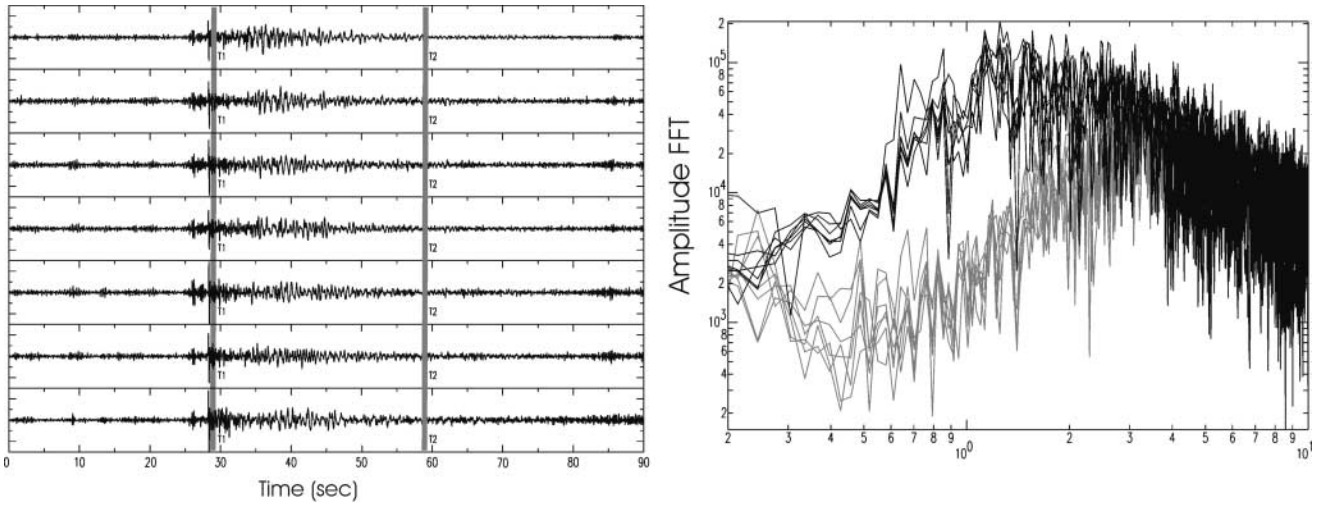

Figure 9. Left: Vertical component of the recorded earthquake. The amplitude scale is normalized for all the seven stations. The 30-sec time window between the T1 and T2 vertical lines was processed. Right: Fourier amplitude spectra for the vertical component of the coda and noise recordings for all the stations (black and gray lines, respectively).

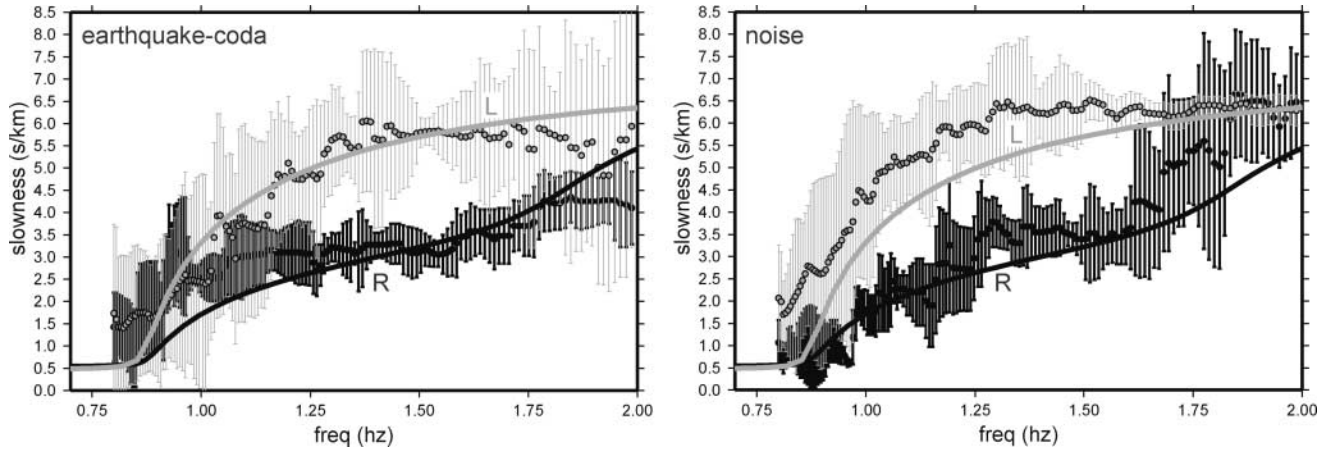

Figure 10. Dispersion curves and their standard deviations for vertical and horizontal motion (black and gray lines, respectively) computed on 30 sec of earthquake coda and noise using CVFK analysis. For the best model in Figure 6 we overlaid the theoretical dispersion curve for the fundamental Rayleigh (R) and Love (L) mode.

ray techniques are employed for deriving shallow shear-wave velocities. In complex-layered sites, such as a lower *S*-wave-velocity layer embedded between higher *S*-wave-velocity layers (Stokoe *et al.*, 1994), higher modes can play a significant role and can hide the fundamental mode within certain frequency bands. Higher modes cannot be easily discriminated using passive techniques alone, because in most cases the passive techniques resolve the low-frequency part of the wave field related to the frequency content of the ambient microtremor. In such cases an integrated approach of passive and multichannel active techniques (i.e., MASW) (Park *et al.*, 1999) could be very useful to increase the accuracy of the dispersion measurements at higher frequency and thus to better identify higher modes. The reliability of the inverted model can be improved by introducing properly identified higher modes in the inversion process (Xia *et al.*, 2003).

In the present article, we show the analysis of ambient vibrations recorded by three-component arrays located in the Colfiorito plain, a small sediment-filled valley. Our aim is to analyze the dispersion characteristics of ambient noise in a test site for which we know fairly well the soil properties and the geometry of the sediment–bedrock interface. The inverted shear-velocity profiles were compared with the available downhole measurements carried out in the central part of the plain (see Fig. 1). Although we used a very simple parameterization (Table 2) we obtain acceptable results (see Fig. 6 and Table 3) in terms of average shear velocity and thickness of the sediment infilling for all the sites that can be approximated as 1D structures (arrays B, B_{large}, D, and E). However, due to the lack of resolution caused by the array geometries, we are not able to reconstruct the fine sediments layering (Fig. 6).

When the situation is far from 1D structure, that is, when 3D effects occur as for array C, the array techniques cannot be applied in such a simple way. For array A that is close to a sag of the bedrock topography (see Fig. 1 and resistivity section of Fig. 8), we obtain ambiguous results: H/V curves exhibit a broader peak (see Fig. 2), and velocities found for the uppermost layers were larger than the ones observed at the other array sites (see Fig. 6, Table 3). These observations for array A were discussed previously by considering a possible role of higher modes of Rayleigh waves (Fig. 8). The *a priori* geophysical and geological information available in the vicinity of array A, as well as the results of noise analysis, indicate a more complex near-surface structure moving toward the southeast edge of the basin.

In general, the good fit between the measured and the theoretical dispersion curves confirms the noise wave field as being mainly composed of surface waves. In Colfiorito, Rayleigh waves are predominant in the vertical plane, while Love waves are propagating in the horizontal plane with a nonnegligible proportion. We find some persistent directions of the wave trains propagating across the arrays that could be explained as local sources within the basin and/or the effects of stable reverberating waves scattered from outcrop edges or linked to the irregularities of the bedrock topography.

After determining soil profiles, we were able to compute the 1D *SH* transfer functions for the sites. Figure 11 shows the 1D transfer functions of the inverted models superimposed on the empirical estimates derived from *S* waves of weak earthquakes using the part of seismograms that should be mainly composed of vertically reverberating body waves. At the fundamental resonance frequency of the sites, the estimated and empirical transfer functions are in good agreement. Interestingly, the estimated transfer function at array B fits also amplification actually observed from weak-motion data at harmonic frequencies, while for array *A* only the amplification at the fundamental resonance frequency is present (see Fig. 11). The lack of amplification at higher frequencies for array A could be explained by (1) destructive

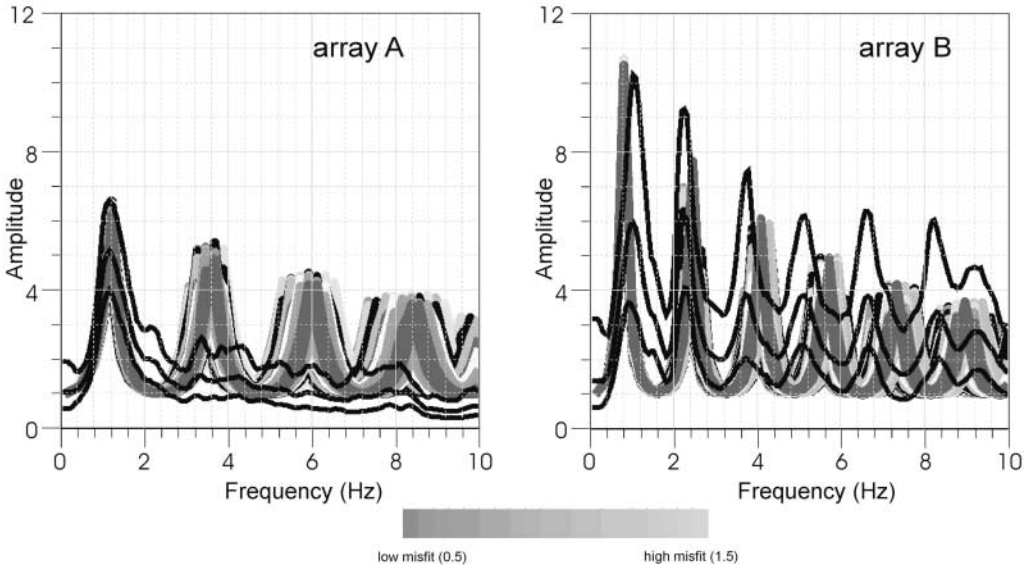

Figure 11. Theoretical versus empirical transfer function for arrays A and B. The average, and the average ± a standard deviation of the classical spectral ratio (black lines) using a reference site (black square in Fig. 1 after Di Giulio *et al.*, 2003) are plotted with 1D transfer functions (vertically incident *SH* waves) for all the inverted models of Figure 6 (gray area). The empirical transfer functions are computed over 51 and 75 local earthquakes for array A and B respectively. The events have a good signal-to-noise ratio in the 0.1- to 10-Hz frequency band and a duration magnitude ranging from 1.9 to 3.7. The window length used in the classical spectral analysis is 10 sec after the *S*-wave arrival. The event data set was collected by stations located near the center of array A and B.

interferences between *S* waves and waves diffracted by the nearby basin edge and/or (2) a very low value of quality factor Q (≤ 5) for the soft upper sediments. If we include the later phases using a larger time window in the classical spectral analysis, the level of amplification around 1 Hz increases by a factor of about 2 (see figure 3 of Di Giulio *et al.* [2003]). Thus the computed 1D theoretical response underestimates the actual amplification in Colfiorito plain since it does not consider 2D and 3D effects, or especially the contribution of basin-edge-induced waves horizontally propagating within the basin (see also Field, 1996; Kawase, 1996; Rovelli *et al.*, 2001; Di Giulio *et al.*, 2003; Cornou and Bard 2003).

Furthermore, the comparison between H/V curves and *SH* transfer functions (Figs. 2 and 11) confirms that the H/V method is only able to provide the fundamental resonance frequency, failing to identify amplifications at higher frequencies.

Additional ongoing experimental and numerical studies in alluvial valleys are in progress (Cornou *et al.*, 2004a,b) to define the potentiality of the noise techniques for different site geometries (1D and 3D, shallow and deep sediment structures) and ambient vibration source characteristics.

Acknowledgments

We thank Fabrizio Cara, Giovanna Cultrera, Danilo Galluzzo, Mario La Rocca, Rosalba Maresca, Gilberto Saccorotti, Alekos Savvaidis, Frank Scherbaum, and Daniel Vollmer for their precious support in the field measurements and in the organization of the experiment. We thank the landowners who kindly gave us permission to install arrays on their property. We also thank Andy Michael and two anonymous reviewers for their constructive criticism that improved the manuscript. We acknowledge Michel Bouchon and D. M. Boore for their comments and encouragement. This study was carried out in the framework of the SESAME project, European Commission, No. EVG1-CT-2000-00026. We are grateful to Pierre-Yves Bard and all the SESAME partners for the ongoing useful discussions.

References

Aki, K. (1969). Analysis of the seismic coda of local earthquakes as scattered waves, *J. Geophys. Res.* **74,** 615–618.

Amato, A., R. M. Azzara, C. Chiarabba, G. B. Cimini, M. Cocco, M. Di Bona, L. Margheriti, S. Mazza, F. Mele, G. Selvaggi, A. Basili, E. Boschi, F. Courboulex, A. Deschamps, S. Gaffet, G. Bittarelli, L. Chiaraluce, D. Piccinini, and M. Ripepe (1998). The 1997 Umbria-Marche, Italy earthquake sequence: a first look at the main shocks and aftershocks, *Geophys. Res. Lett.* **25,** 2861–2864.

Arai, H., and K. Tokimatsu (2004). *S*-wave velocity profiling by inversion of microtremor H/V spectrum, *Bull. Seism. Soc. Am.* **94,** 53–63.

Asten, M. W., and D. M. Boore (2005). Comparison of shear-velocity profiles of unconsolidated sediments near the Coyote borehole (CCOC) measured with fourteen invasive and non-invasive methods, in *Blind Comparisons of Shear-Wave Velocities at Closely-Spaced Sites in San Jose, California,* M. W. Asten and D. M. Boore (Editors), *U.S. Geol. Surv. Open-File Rept.* http://pubs.usgs.gov/of/2005/1169/ (last accessed August 2006).

Asten, M. W., and J. D. Henstridge (1984). Array estimators and the use of microseisms for reconnaissance of sedimentary basins, *Geophysics* **49,** 1828–1837.

Bard, P.-Y., and M. Bouchon (1985). The two-dimensional resonance of sediment-filled valleys, *Bull. Seism. Soc. Am.* **75,** no. 2, 519–541.

Bonnefoy-Claudet, S. (2004). Nature du brut de fond sismique: implications pour les études des effets de site, *Ph.D. Thesis,* Joseph Fourier University, Grenoble, France, 216 pp. (in French).

Brown, L. T., D. M. Boore, and K. H. Stokoe, II (2002). Comparison of shear-wave slowness profiles at 10 strong-motion sites from noninvasive SASW measurements and measurements made in boreholes, *Bull. Seism. Soc. Am.* **92,** no. 8, 3116–3133.

Building Seismic Safety Council (BSSC) (2001). NEHRP recommended provisions for seismic regulations for new buildings and other structures, 2000 Edition, Part 1: Provisions, prepared by the Building Seismic Safety Council for the Federal Emergency Management Agency, Report FEMA 368, Washington, D.C.

Capon, J. (1969). High-resolution frequency–wavenumber spectrum analysis, *Proc. IEEE*, **57,** no. 8, 1408–1418.

Cara, F., G. Di Giulio, and A. Rovelli (2003). A study on seismic noise variations at Colfiorito, Central Italy: implications for the use of H/V spectral ratios, *Geophys. Res. Lett.* **30,** no. 18, 1972, doi 10.1029/2003GL017807.

Chiaraluce, L., M. Barchi, C. Collettini, F. Mirabella, and S. Pucci (2005). Connecting seismically active normal faults with Quaternary geological structures in a complex extensional environment: the Colfiorito 1997 case history (northern Apennines, Italy), *Tectonics* **24,** TC1002, doi 10.1029/2004TC001627.

Cornou, C., and P.-Y. Bard (2003). Site-to-bedrock over 1D transfer function ratio: an indicator of the proportion of edge-generated surface waves? *Geophys. Res. Lett.* **30,** no. 9, 1453, doi 10.1029/2002GL016593.

Cornou, C., P.-Y. Bard, and M. Dietrich (2003). Contribution of dense array analysis to identification an quantification of basin-edge-induced waves, Part I: Methodology, *Bull. Seism. Soc. Am.* **93,** no. 6, 2604–2623.

Cornou, C., J. Kristek, M. Ohrnberger, G. Di Giulio, E. Schisselé, B. Guillier, S. Bonnefoy-Claudet, M. Wathelet, D. Fäh, P. Y. Bard, and M. Moczo (2004a). Simulation of seismic ambient vibrations—II H/V and array techniques for real sites, *Proc. 13th World Conference on Earthquake Engineering,* Vancouver B.C., 1–6 August 2004, paper no. 1130.

Cornou, C., and SESAME Group (2004b). Simulation for real sites: set of noise synthetics for H/V and array studies from simulation of real sites and comparison for test sites, SESAME report D11.10 and D17.10, http://sesame-fp5.obs.ujf-grenoble.fr (last accessed August 2006).

Di Giulio, G., A. Rovelli, F. Cara, R. M. Azzara, F. Marra, R. Basili, and A. Caserta (2003). Long-duration asynchronous ground motions in the Colfiorito plain, central Italy, observed on a two-dimensional dense array, *J. Geophys. Res.* **108,** no. B10, 2486, doi 10.1029/2002JB002367.

Dobry, R., R. D. Borcherdt, C. B. Crouse, I. M. Idriss, W. B. Joyner, G. R. Martin, M. S. Power, E. E. Rinne, and R. B. Seed (2000). New site coefficients and site classification system used in recent buildings seismic code provisions, *Earthquake Spectra* **16,** 41–67.

Fäh, D., F. Kind, and D. Giardini (2001). A theoretical investigation of average H/V ratios, *Geophys. J. Int.* **145,** 535–549.

Fäh, D., F. Kind, and D. Giardini (2003). Inversion of local S-wave velocity structures from average H/V ratios, and their use for the estimation of site-effects, *J. Seism.* **7,** 449–467.

Field, E. H. (1996). Spectral amplification in a sediment-filled valley exhibiting clear basin-edge-induced waves, *Bull. Seism. Soc. Am.* **86,** 991–1005.

Forbriger, T. (2003). Inversion of shallow-seismic wavefields I. Wavefield transformation, *Geophys. J. Int.* **153,** 719–734.

Jin, X., B. Luke, and J. Louie (2006). Comparison of Rayleigh wave dispersion relations from three surface wave measurements in a complex-layered system, in *Proc. GeoCongress 2006: Geotechnical Engineering in the Information Technology Age*, Atlanta 26 February-1 March 2006.

Kawase, H. (1996). The cause of the damage belt in Kobe: "The Basin-Edge Effect" constructive interference of the direct S-wave with the basin-induced diffracted/Rayleigh waves, *Seism. Res. Lett.* **67,** no. 5, 25–34.

Kind, F. (2002). Development of microzonation methods: application to Basle, Switzerland, *Ph.D. Thesis*, Swiss Federal Institute of Technology, Zurich, Switzerland.

Konno, K., and T. Ohmachi (1998). Ground motion characteristics estimated from spectral ratio between horizontal and vertical components of microtremor, *Bull. Seism. Soc. Am.* **88,** no. 1, 228–241.

Kvaerna, T., and F. Ringdahl (1986). Stability of various *f-k* estimation techniques, Semiannual Technical Summary, NORSAR Scientific Report, 29–40.

Horike, M. (1985). Inversion of phase velocity of long-period microtremors to the S-wave-velocity structure down to the basement in urbanized areas, *J. Phys. Earth.* **33,** 59–96.

Lachet, C., and P. Y. Bard (1994). Numerical and theoretical investigations on the possibilities and limitation of the Nakamura technique, *J. Phys. Earth*. **42,** 377–397.

Lermo, J., and F. J. Chàvez-Garcia (1993). Site evaluation using spectral ratios with only one station, *Bull. Seism. Soc. Am.* **83,** 1574–1594.

Malischewsky, P. G., and F. Scherbaum (2004). Love's formula and H/V-ratio (ellipticity) of Rayleigh waves, *Wave Motion* **40,** 57–67.

Maresca, R., D. Galluzzo, and E. Del Pezzo (2006). H/V spectral ratios and array techniques applied to ambient noise recorded in the Colfiorito basin, central Italy, *Bull. Seism. Soc. Am.* **96**, 490–505.

Nakamura, Y. (1989). A method for dynamic characteristics estimation of subsurface using microtremor on the ground surface, *Q. Rep. Railway Tech. Res. Inst.* **30,** no. 1, 25–33.

Nakamura, Y. (2000). Clear identification of fundamental idea of Nakamura's technique and its applications, in *Proc. 12th World Conference on the Earthquake Engineering*, Auckland, New Zealand.

Nogoshi, M., and T. Igarashi (1971). On the amplitude characteristic of microtremor (part 2) (in Japanese with English abstract), *J. Seism. Soc. Japan* **24,** 26–40.

Ohrnberger, M. (2004). User manual for software package CAP—a continuous array processing toolkit for ambient vibration array analysis, SESAME report D18.06, http://sesame-fp5.obs.ujfgrenoble.fr, (last accessed August 2006).

Ohrnberger, M., E. Schisselé, C. Cornou, M. Wathelet, A. Savvaidis, F. Scherbaum, D. Jongmans, and F. Kind (2004a). Microtremor array measurements for site effect investigations: comparison of analysis methods for field data crosschecked by simulated wavefields, in *Proc. 13th World Conference on Earthquake Engineering*, Vancouver, B.C., Canada, 1–6 August 2004, paper no. 0940.

Ohrnberger, M., E. Schisselé, C. Cornou, S. Bonnefoy-Claudet, M. Wathelet, A. Savvaidis, F. Scherbaum, and D. Jongmans (2004b). Frequency wavenumber and spatial autocorrelation methods for dispersion curve determination from ambient vibration recordings, in *Proc. 13th World Conference on Earthquake Engineering*, Vancouver, B.C., Canada, 1–6 August 2004, paper no. 0946.

Park, C. B., R. D. Miller, and J. Xia (1999). Multi-channel analysis of surface waves (MASW), *Geophysics* **64,** 800–808.

Parolai, S., M. Picozzi, S. M. Richwalski, and C. Milkereit (2005). Joint inversion of phase velocity dispersion and H/V ratio curves from seismic noise recordings using a genetic algorithm, considering higher modes, *Geophys. Res. Lett.* **32,** LO1303, doi 10.1029/2004GL021115.

Rial, J. A. (1989). Seismic wave resonances in 3-D sedimentary basin, *Geophys. J. Int.* **99,** 81–90.

Roten, D., C. Cornou, S. Steimen, D. Fäh, and D. Giardini (2004). 2D resonances in alpine valleys from ambient vibration wavefield, in *Proc. 13th World Conference on Earthquake Engineering*, Vancouver B.C., Canada, 1–6 August 2004, paper no. 0845.

Rovelli, A., L. Scognamiglio, F. Marra, and A. Caserta (2001). Edge-diffracted 1-s surface waves observed in a small-size intermontane basin (Colfiorito, central Italy), *Bull. Seism. Soc. Am.* **91,** 1851–1866.

Sambridge, M. (1999). Geophysical inversion with a neighbourhood al-

gorithm I. Searching a parameter space, *J. Geophys. Res.* **103,** 4839–4878.

Scherbaum, F., K.-G. Hinzen, and M. Ohrnberger (2003). Determination of shallow shear wave velocit profiles in the Cologne, Germany area using ambient vibrations, *Geophys. J. Int.* **152,** no. 3, 597–612.

Schisselé, E., J. Guilbert, Y. Cansi, and S. Gaffet (2004). Accurate time-frequency-wavenumber analysis to study coda waves, *Geophys. J. Int.* **158,** no. 2, 577–591.

Site Effects using Ambient Excitations (SESAME) (2001–2004). http://sesame-fp5.obs.ujf-grenoble.fr (last accessed August 2006).

Stokoe, K. H., II, S. G. Wright, J. A. Bay, and J. M. Roësset (1994). Characterization of geotechnical sites by SASWS method, in *Geophysical Characterization of Sites, ISSMFE Technical Committee # 10*, R. D. Woods (Editor), Oxford Publishers, New Delhi, 15–25.

Tokimatsu, K., K. Shinzawa, and S. Kuwayama (1992). Use of short-period microtremors for vs profiling, *J. Geotech. Eng. ASCE* **118,** no. 10, 1554–1558.

Tokimatsu, K. (1997). Geothermal site characterization using surface waves, in *Earthquake Geotechnical Engineering*, K. Ishihara (Editor), Balkema, Rotterdam, 1333–1368.

Wathelet, M. (2005). Array recordings of ambient vibrations: surface-waves inversion, *Ph.D. Thesis,* University of Liege, Belgium, 177 pp.

Wathelet, M., D. Jongmans, and M. Ohrnberger (2004). Surface wave inversion using a direct search algorithm and its application to ambient vibrations measurements, *Near Surface Geophys.* **2,** 211–221.

Woods, J. W., and P. R. Lintz (1973). Plane waves at small arrays, *Geophysics* **38,** no. 6, 1023–1041.

Xia, J., R. D. Miller, and C. B. Park (1999). Estimation of near-surface shear-wave velocity by inversion of Rayleigh waves, *Geophysics* **64,** no. 3, 691–700.

Xia, J., R. D. Miller, C. B. Park, and G. Tian (2003). Inversion of high frequency surface waves with fundamental and higher modes, *J. Appl. Geophys.* **52,** no. 1, 45–57.

Zerva, A., and O. Zhang (1996). Estimation of signal characteristics in seismic ground motion, *Probabilistic Eng. Mech.* **11,** 229–242.

Zywicki, D. J. (1999). Advanced signal processing methods applied to engineering analysis of seismic surface waves, *Ph.D. Thesis,* Georgia Institute of Technology, Atlanta.

Istituto Nazionale di Geofisica e Vulcanologia,
Via Castello d'Aquino 13
Grotttaminarda, 83035, Avellino, Italy
(G.D.G.)

Laboratoire de Géophysique Interne et Tectonophysique (LGIT/IRD),
Maison des Geosciences
BP53, 38041 Grenoble Cédex 9
Grenoble, France
(C.C.)

Institut für Geowissenschaften, Universität Potsdam (IGUP)
Karl-Liebknecht-Strasse 24
D-14476 Golm, Potsdam, Germany
(M.O.)

GEOMAC, University of Liège,
1 Chemin des Chevreuils, B52
4000 Liege, Belgium
(M.W.)

Istituto Nazionale di Geofisica e Vulcanologia,
Via di Vigna Murata 605
00143 Rome, Italy
(A.R.)

Manuscript received 21 March 2005.